

# On proton synchrotron blazar models: the case of quasar 3C 279

M. Petropoulou (MP) <sup>\*</sup> and A. Mastichiadis (AP) <sup>†</sup>

*Department of Physics, University of Athens, Panepistimiopolis, GR 15783 Zografos, Greece*

Received.../Accepted...

## ABSTRACT

In the present work we propose an innovative estimation method for the minimum Doppler factor and energy content of the  $\gamma$ -ray emitting region of quasar 3C 279, using a standard proton synchrotron blazar model and the principles of automatic photon quenching. The latter becomes relevant for high enough magnetic fields and results in spontaneous annihilation of  $\gamma$ -rays. The absorbed energy is then redistributed into electron-positron pairs and soft radiation. We show that as quenching sets an upper value for the source rest-frame  $\gamma$ -ray luminosity, one has, by necessity, to resort to Doppler factors that lie above a certain value in order to explain the TeV observations. The existence of this lower limit for the Doppler factor has also implications on the energetics of the emitting region. In this aspect, the proposed method can be regarded as an extension of the widely used one for estimating the equipartition magnetic field using radio observations. In our case, the leptonic synchrotron component is replaced by the proton synchrotron emission and the radio by the VHE  $\gamma$ -ray observations. We show specifically that one can model the TeV observations by using parameter values that minimize both the energy density and the jet power at the cost of high-values of the Doppler factor. On the other hand, the modelling can also be done by using the minimum possible Doppler factor; this, however, leads to a particle dominated region and high jet power for a wide range of magnetic field values. Despite the fact that we have focused on the case of 3C 279, our analysis can be of relevance to all TeV blazars favoring hadronic modelling that have, moreover, simultaneous X-ray observations.

**Key words:** astroparticle physics – radiation mechanisms: non-thermal – gamma rays: galaxies – galaxies: active

## 1 INTRODUCTION

Blazars, a subclass of Active Galactic Nuclei, emit non-thermal, highly variable radiation across the whole electromagnetic spectrum. According to the standard scenario, particles accelerate to relativistic energies in the jets of these objects which point, within a small angle, towards our direction and the resulting photon emission is boosted due to relativistic beaming.

Detailed modelling of observations, especially in the  $\gamma$ - and X-ray regimes, makes possible the estimation of the physical parameters of the emitting region. Thus quantities like the source size, the magnetic field strength, the bulk Lorentz factor and the particle energy density can nowadays be routinely calculated. Furthermore, from the values of these quantities one could obtain meaningful estimates

for the particle and Poynting fluxes and use them to make comparisons, for example, to the Eddington luminosity of the source, connecting thus the black hole energetics with the jet power.

One major uncertainty of the modelling is the nature of the radiating particles. While there seems to be a consensus that the emission from radio to X-rays comes from the synchrotron radiation of a population of relativistic electrons, there are still open questions regarding the  $\gamma$ -ray emission of these objects. Broadly speaking, the models fall into two categories, the leptonic ones (e.g. Dermer, Schlickeiser, & Mastichiadis 1992; Maraschi, Ghisellini, & Celotti 1992; Dermer & Schlickeiser 1993) which assume that the same electrons which radiate at lower frequencies via synchrotron produce the  $\gamma$ -rays by inverse Compton scattering and the hadronic ones (Mannheim & Biermann 1992; Mücke & Protheroe 2001; Böttcher, Reimer, & Marscher 2009; Mücke et al. 2003) which postulate that an extra population of relativistic pro-

<sup>\*</sup> E-mail: maroulaaki@gmail.com

<sup>†</sup> E-mail: amastich@phys.uoa.gr

tons produce the high energy radiation as a result of hadronically induced and electromagnetic processes.

Due to the very different radiating mechanisms involved, the two classes of models can result in very different parameters for the source. Thus, for example, typical leptonic synchrotron self-compton models require low magnetic field strengths, ranging from  $B \simeq 0.01 - 1$  G for high synchrotron-peaked BL Lacs (Tavecchio et al. 2011; Murase et al. 2012) up to  $B \simeq 1 - 10$  G for Flat Spectrum Radio Quasars, and low jet power ( $\simeq 10^{47}$  erg/sec) (e.g. Celotti & Ghisellini 2008). On the other hand, the corresponding values for the hadronic models are higher by at least one order of magnitude (e.g. Protheroe & Mücke 2001; Böttcher et al. 2009). While both can fit reasonably well the observations, they both face some problems. For instance, it has been argued that one problem with leptonic models is the high ratio between the required relativistic electron energy density to the magnetic one, implying large departures from equipartition. On the other hand, the hadronic models imply jet powers which can be uncomfortably high, especially when compared to the accretion luminosity.

In previous work (Petropoulou & Mastichiadis 2012) we have argued that automatic  $\gamma$ -ray quenching, i.e. a loop of processes which result in spontaneous  $\gamma$ -ray absorption accompanied by production of electron-positron pairs and soft radiation, can become instrumental in the modelling of high energy sources. Its application to any  $\gamma$ -ray emitting region, makes it relevant to both leptonic and hadronic models; the fact, however, that quenching requires rather high magnetic fields makes it more relevant for the latter. In the present paper we revisit the hadronic model taking into account the effects of non-linear photon quenching. This, as we shall show, has as a result to exclude many sets of parameters, which otherwise would give good fits to observations, as the non-linear cascade growth modifies drastically the produced multiwavelength spectrum.

As a typical example we focus on the quasar 3C 279. This has been detected for the first time in very high-energy (VHE)  $\gamma$ -rays at  $> 100$  GeV by the MAGIC telescope (Albert et al. 2008) and ever since it remains the most distant VHE  $\gamma$ -ray source with a well measured redshift. Both leptonic and (lepto)hadronic models have been applied (Böttcher et al. 2009) and it has been pointed out that the former require the system to be well out of equipartition.

In the present work we fit only the VHE part of the spectrum using a proton-synchrotron blazar model and use the contemporary X-ray data (see e.g. Chatterjee et al. (2008)) as an upper limit; the modelling of the complete multiwavelength spectrum requires a primary leptonic population radiating in the IR/X-ray energy bands which, we assume, that can always be determined. We show that one can derive a lower limit for the Doppler factor of the radiating blob by just combining (i) the values of the proton luminosity and the Doppler factor for a given magnetic field that provide a good fit to the MAGIC data and (ii) the fact that for high values of the proton injection compactness the absorption of  $\gamma$ -rays becomes non-linear leading to an overproduction of softer photons and consequently violating the X-ray observations *even in the absence of a leptonic component*. We also show that the minimum possible value of the Doppler factor is largely independent of the magnetic field and this

has some interesting implications for the energetics of 3C 279.

The paper is structured as follows. In §2 we give some simple, qualitative estimates on the effects of quenching on fitting the multiwavelength data of blazars, in §3 we apply these, using a numerical code, to the case of 3C 279 and we conclude in §4 with a discussion of our results. For numerical results we adopt working in the  $\Lambda$ CDM cosmology with  $H_0 = 70$  km s $^{-1}$  Mpc $^{-1}$ ,  $\Omega_m = 0.3$  and  $\Omega_\Lambda = 0.7$ . The redshift of 3C 279  $z = 0.536$  corresponds to a luminosity distance  $D_L = 3.08$  Gpc.

## 2 ANALYTICAL ESTIMATES BASED ON AUTOMATIC QUENCHING

In this section we will justify the existence of a minimum Doppler factor using analytical expressions in the simplest possible framework. The functional dependence of various physical quantities on the magnetic field strength, such as the particle density and the observed jet power, will also be derived.

We consider a spherical blob of radius  $R$  moving with a Doppler factor  $\delta$  with respect to us and containing a magnetic field of strength  $B$ . We further assume that ultra-relativistic protons with a power law distribution of index  $s$  are being constantly injected into the source with a rate given by

$$\dot{Q}_p = \tilde{Q}_{po} \gamma_p^{-s} H(\gamma_p - \gamma_{\min}) H(\gamma_{\max} - \gamma_p), \quad (1)$$

where  $\gamma_{\min}$  and  $\gamma_{\max}$  are the lower and upper limits of the injected distribution respectively and  $H(x)$  is the Heaviside function.  $\tilde{Q}_{po}$  is the normalization constant and is also directly related to the proton injection compactness as:

$$\ell_p = \tilde{Q}_{po} m_p c^2 \frac{\sigma_T R}{3t_{cr}} \frac{\gamma_{\min}^{-s+2} - \gamma_{\max}^{-s+2}}{2-s}, \quad (s \neq 2). \quad (2)$$

or

$$\ell_p = \tilde{Q}_{po} m_p c^2 \frac{\sigma_T R}{3t_{cr}} \ln \left( \frac{\gamma_{\max}}{\gamma_{\min}} \right), \quad (s = 2), \quad (3)$$

where  $t_{cr} = R/c$ . This can be further related to the proton injected luminosity by the relation

$$L_p = \frac{4\pi R m_p c^3}{\sigma_T} \ell_p, \quad (4)$$

where  $\sigma_T$  is the Thomson cross section.

Protons will lose energy by synchrotron radiation, photopair and photopion processes as has been described in Petropoulou & Mastichiadis (2012) and therefore the proton distribution function is given by the solution of a time-dependent kinetic equation that includes particle injection in the form of equation (1) in addition to particle losses and escape. Furthermore, since the loss processes will create photons and electrons, one has to follow the evolution of these two species by writing two additional kinetic equations for them. The solution of the system of the resulting three coupled partial integrodifferential equations gives the corresponding particle distribution functions and the multiwavelength photon spectra can be calculated in a straightforward manner. The picture above is rather complicated and it can be treated only numerically (see section 3).

In the case, however, where the cooling of protons does

not play a significant role in comparison to particle escape, the steady-state proton number density is then simply given by

$$n_p(\gamma) = t_{cr} \tilde{Q}_{po} \gamma^{-s}, \text{ for } \gamma_{min} \leq \gamma \leq \gamma_{max}, \quad (5)$$

where we have assumed that the proton escape timescale equals the crossing timescale. Moreover, since we fit only the VHE  $\gamma$ -rays and not the whole multiwavelength spectrum, there is no need in calculating the evolution of the secondary leptons that will radiate at lower energies. MAGIC data lie above  $10^{25}$  Hz. The  $\gamma$ -ray spectrum in  $\nu F_\nu$  peaks at  $\epsilon_\gamma^{obs} = 100$  GeV or equivalently at frequency  $\nu_\gamma^{obs} = 2 \times 10^{25}$  Hz<sup>1</sup>, which we will try to fit with the proton synchrotron spectrum emitted by the particle distribution of equation (5). We will focus on the case where the distribution of protons is not cooled and the synchrotron spectrum peaks at the maximum synchrotron energy, which implies that  $t_{cool}(\gamma_{max}) \leq t_{cr}$ . Thus, our analysis is valid under the prerequisite

$$B^2 \gamma_{max} \lesssim 10^{-3} R \text{ in cgs.} \quad (6)$$

In this framework we obtain our first relation

$$\epsilon_\gamma^{obs} = C_1 \delta B \gamma_{max}^2, \quad (7)$$

where  $\epsilon_\gamma^{obs} = h\nu_\gamma^{obs}$  and  $C_1 = \hbar e/m_p c(1+z)$ . The total synchrotron power per frequency in the blob frame for the proton distribution of equation (5) is given by

$$P_\nu = C_2 N_p B^{\frac{s+1}{2}} \nu^{-\frac{s-1}{2}}, \quad (8)$$

where

$$C_2 \approx \frac{2e^{7/2}}{\sqrt{6\pi} m_p^{3/2} c^{5/2}} \quad (9)$$

and  $N_p$  is the total number of radiating protons in the blob, which is given by  $N_p = t_{cr} V \tilde{Q}_{po} (1/\gamma_{min} - 1/\gamma_{max}) \approx t_{cr} V \tilde{Q}_{po}$ , where the approximation  $\gamma_{max}^{-1} \ll 1$  has been made; here we have used also  $\gamma_{min} = 1$  and  $s = 2$ . This can also be expressed in terms of proton energy density  $u_p$  as

$$N_p = \frac{u_p V}{\ln(\gamma_{max}) m_p c^2}. \quad (10)$$

In the above expressions  $V \approx \pi R^3$  is the volume of the spherical blob.

## 2.1 Derivation of the minimum Doppler factor

By combining equation (7) with the integrated power over all synchrotron frequencies (equation 8) one obtains the total comoving synchrotron power

$$L = 2C_2 N_p (\nu_\gamma^{obs})^{1/2} B^{3/2} \delta^{-1/2} \quad (11)$$

that is related to the total observed  $\gamma$ -ray luminosity  $L_\gamma^{obs} \approx 10^{48}$  erg/s by the usual relation  $L_\gamma^{obs} = \delta^4 L$ . This leads to our second relation

$$L_\gamma^{obs} = C_2' u_p B^{3/2} \delta^{7/2}, \quad (12)$$

<sup>1</sup> Throughout the present work quantities with the index ‘obs’ will refer to the observer’s frame, whereas all other quantities refer to the blob frame.

where  $C_2' = 2C_2 V (\nu_\gamma^{obs})^{1/2} / \ln(\gamma_{max}) m_p c^2$ . For a specific magnetic field we find a relation of proportionality

$$\delta \propto u_p^{-2/7} \propto \ell_p^{-2/7}, \quad (13)$$

which is also verified by the detailed numerical treatment (see section 3.2). We note that the proportionality at the right hand side of relation (13) holds only if the magnetic field is not strong enough to cause significant proton cooling due to synchrotron radiation.

The maximum proton Lorentz factor has remained so far undetermined. However, the fact that the proton gyroradius  $r_g$  should be less or equal than the size of the blob  $R$  (Hillas 1984) sets a strong upper limit

$$\gamma_{max} = \kappa \frac{eBR}{m_p c^2}, \quad (14)$$

where  $\kappa$  is a scaling factor that takes values less or equal to unity. It has been introduced in order to take into account the fact, that good fits can be obtained for certain parameter sets with  $\gamma_{max} \ll eBR/m_p c^2$ ; as an example see the parameters used for figure 4. By combining the above relation with equation (7) we find a lower limit for the Doppler factor

$$\delta \geq \delta_{min} = C_3 B^{-3}, \quad (15)$$

where

$$C_3 = \frac{1}{C_1} \left( \frac{m_p c^2}{\kappa e} \right)^2 \frac{\epsilon_\gamma^{obs}}{R^2}. \quad (16)$$

Automatic quenching of  $\gamma$ -rays was irrelevant to the derivation of the relations presented up to this point. Actually, it will not play any role in the evolution of the system if the magnetic field is weak enough. There is, in other words, a necessary but not sufficient condition for the operation of automatic quenching, the so-called *feedback criterion*. This can be derived from the requirement that the magnetic field is strong enough so that the synchrotron photons of the automatically produced pairs lie above the threshold for further photon-photon absorption on the  $\gamma$ -rays (Stawarz & Kirk 2007; Petropoulou & Mastichiadis 2011, 2012). This requirement sets a lower limit for the magnetic field

$$B \geq 8B_{cr} \left( \frac{m_e c^2}{\epsilon_\gamma} \right)^3, \quad (17)$$

where  $B_{cr} = 4.4 \times 10^{13}$  G. If we set  $\epsilon_\gamma = \epsilon_\gamma^{obs} (z+1) \delta^{-1}$  and use equations (7) and (14) we find an expression for the magnetic field  $B_q$ , below which the feedback criterion is not satisfied. This involves only physical constants except for the size of the blob  $R$  and the scaling factor  $\kappa$ :

$$B_q = (8B_{cr})^{1/10} \left( \frac{m_p m_e c^3}{\hbar e} \right)^{3/10} \left( \frac{m_p c^2}{e \kappa R} \right)^{3/5}. \quad (18)$$

In order to have an estimate, the above expression gives  $B_q \approx 3.5$  G for  $R = 3 \times 10^{16}$  cm and  $\kappa = 1$ . Note that for a given  $R$  this is also the minimum value of  $B_q$ . One could also express  $B_q$  in terms of  $\gamma_{max}$  as

$$B_q = (8B_{cr})^{1/4} \left( \frac{m_p m_e c^3}{\hbar e} \right)^{3/4} \gamma_{max}^{-3/2}, \quad (19)$$

as long as  $\gamma_{max}$  does not exceed the value given by equation (14) for  $\kappa = 1$ . From equation (12) becomes evident that if

the Doppler factor decreases then the proton energy density or the proton compactness equivalently should increase in order to obtain the same observed luminosity. If, however, the feedback criterion is satisfied, then the proton compactness is bounded from above. This immediately sets a lower limit for the Doppler factor. We proceed next to obtain an expression of  $\delta_{\min}$ . In previous work we have obtained an analytical expression for the critical  $\gamma$ -ray compactness (see equation (34) of Petropoulou & Mastichiadis (2011)), which will prove very useful for our analytical calculations

$$\ell_{\text{cr}}^{\text{inj}} \approx C_4 B^{1/2} \delta^{-1/2}, \quad (20)$$

where  $C_4 = (2\epsilon_\gamma^{\text{obs}}/\sigma_0^2 B_{\text{cr}} m_e c^2)^{1/2}$  and  $\sigma_0 = 4/3$  is a normalization constant. The  $\gamma$ -ray compactness is defined as  $\ell_\gamma = L\sigma_{\text{T}}/4\pi R m_e c^3$ . Using equation (11) expressed in terms of proton compactness  $\ell_p$  instead of total proton number  $N_p$  we can rewrite the above definition as

$$\ell_\gamma = C_5 \ell_p B^{3/2} \delta^{-1/2}, \quad (21)$$

where

$$C_5 = \frac{6C_2 V (\nu_\gamma^{\text{obs}})^{1/2}}{4\pi R^2 m_e c^3 \ln(\gamma_{\text{max}})}. \quad (22)$$

In order to avoid an overproduction of soft photons that would violate the upper limit set by the X-ray observations we require that  $\ell_\gamma \leq \lambda \ell_{\text{cr}}^{\text{inj}}$ , where  $\lambda$  is a numerical factor between 1 and 10; the exact value can be estimated only numerically. This requirement defines a maximum proton compactness

$$\ell_{p,\text{max}} = \lambda \frac{C_4}{C_5} B^{-1}, \quad (23)$$

which, if inserted in equation (12), gives the minimum Doppler factor

$$\delta_{\min} = \left( \frac{L_\gamma^{\text{obs}} \sigma_{\text{T}}}{4\pi R \lambda m_e c^3 C_4} \right)^{2/7} B^{-1/7}. \quad (24)$$

We note that  $\delta_{\min}$  given by the equation above is a rather robust limit, since it depends weakly on the physical quantities. We note also that the numerical factor  $\lambda$  appears in the above expression raised to the power  $-2/7$  and therefore it does not affect the value of  $\delta_{\min}$  severely.

Summarizing, we have found that for  $B < B_q$ , the minimum value of the Doppler factor is defined by the requirement that the gyroradius is less than the blob size and it has a very strong dependence on the magnetic field, i.e.  $\delta_{\min} \propto B^{-3}$ . On the other hand, for  $B \geq B_q$ , it is defined by the requirement that the proton compactness cannot exceed a critical value. The dependence on the magnetic field is in this case weak, i.e.  $\delta_{\min} \propto B^{-1/7}$ .

## 2.2 Conditions for equipartition

Estimations of the equipartition magnetic field of a relativistically moving blob are common in the literature and are based on fitting the low-frequency synchrotron spectrum of a power-law distribution electrons to radio observations (Pacholczyk 1970). Here we derive an expression for the equipartition magnetic field in a proton-synchrotron blazar model, replacing the power-law distribution of electrons with protons and the radio with VHE  $\gamma$ -ray observations. From

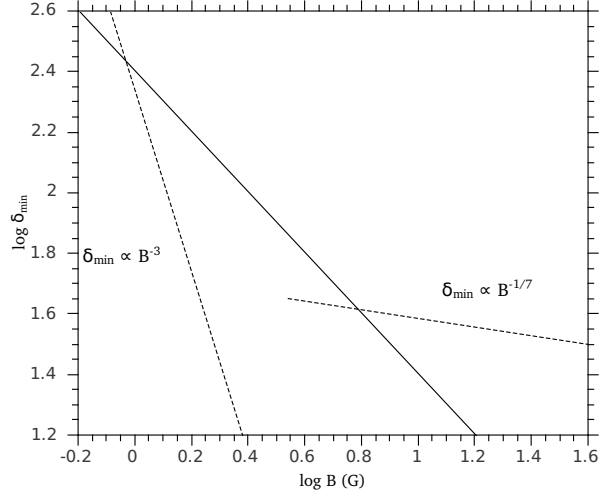


**Figure 1.** Minimum Doppler factor as a function of  $B$  (dashed lines) and locus of points satisfying the equipartition condition (solid line) for  $L_\gamma^{\text{obs}} = 10^{48}$  erg/s,  $\nu_\gamma^{\text{obs}} = 2 \times 10^{25}$  Hz,  $R = 3 \times 10^{16}$  cm and  $\lambda = 5$ .

equation (12) we find that the comoving proton energy density is given by

$$u_p = AB^{-3/2} \delta^{-7/2}, \quad (25)$$

where  $A = L_\gamma^{\text{obs}} C_2'^{-1}$ . Assuming that the energy density of secondary leptons is negligible with respect to that of protons, we can compute the equipartition field  $B_{\text{eq}}$

$$B_{\text{eq}} = (8\pi A)^{2/7} \delta^{-1} \quad (26)$$

or

$$B_{\text{eq}} = 718 L_{\gamma,48}^{\text{obs}} R_{16}^{-6/7} (\nu_{\gamma,25}^{\text{obs}})^{-1/7} \ln(\gamma_{\text{max},10}) \delta^{-1} \quad \text{in G.} \quad (27)$$

We note that here and in what follows the convention  $Q_X \equiv Q/10^X$  in cgs units was adopted unless stated otherwise. The above expression apart from the numerical constant, is identical to that found using equipartition arguments in the context of a leptonic model (see e.g. equation (A7) of Harris & Krawczynski (2002)). In the previous subsection it was found that the Doppler factor of the blob has a minimum value  $\delta_{\min}$  and its functional dependence on  $B$  was also derived. One can therefore investigate whether or not the system can achieve equipartition under the requirement that  $\delta = \delta_{\min}$  and in this case estimate  $B_{\text{eq}}$  using equation (27).

Figure 1 shows  $\delta_{\min}(B)$  given by equations (15) and (24) and the line  $\delta \propto B_{\text{eq}}$  for  $R = 3 \times 10^{16}$  cm and  $\lambda = 5$ . The discontinuity occurs at  $B_q$ , where the functional dependence of  $\delta_{\min}$  on  $B$  changes. The expressions derived should not be trusted in the neighbourhood of  $B_q$ . The points of intersection correspond to the equipartition magnetic field values. The physical system can be found in equipartition either moving with a high Doppler factor and being weakly magnetized or moving with a modest Doppler factor and containing a stronger magnetic field.

A robust result of our treatment, which also differentiates it from other works, is that for a given magnetic field there is a minimum value for the Doppler factor of the flow that is set either by the gyroradius or by automatic quench-

ing arguments. Whenever the analysis of a physical problem leads in the derivation of an extremum for some parameter, it is interesting to study the properties of the physical system in this case. For this reason, in the following we present how the particle energy density and the power of the jet depend on the magnetic field in the particular case of  $\delta = \delta_{\min}$ . Using equations (15), (24) and (25) we find that

$$u_p(\delta_{\min}(B)) \equiv u_p^* \propto B^9 \quad \text{for } B < B_q \quad (28)$$

and

$$u_p(\delta_{\min}(B)) \equiv u_p^* \propto B^{-1} \quad \text{for } B > B_q. \quad (29)$$

Note the large change in the dependence of the proton energy density on  $B$ . The last proportionality is not valid for very high values of the magnetic field, since in this case the synchrotron cooling becomes important and is against our initial assumptions.

### 2.3 Jet power estimates

In an one-zone homogeneous model the emitting plasma is confined in a blob with radius  $R$  moving with a velocity  $\beta c$  and bulk Lorentz factor  $\Gamma$  at an angle  $\theta$  with respect to the line of sight. The radiation is further assumed to originate from a region in the jet of volume  $V \approx \pi R^3$ . The energy densities of particles, magnetic field and radiation are contributing to the jet power. Using the approximations  $\theta \approx 1/\Gamma$ ,  $\delta \approx \Gamma$  and  $\beta \approx 1$  the observed jet power is given by

$$P_{\text{jet}}^{\text{obs}} = \pi R^2 \delta^2 \beta c (u_B + u_{\text{part}} + u_{\text{rad}}), \quad (30)$$

where  $u_{\text{part}} \approx u_p$ ,  $\beta = \sqrt{1 - 1/\Gamma^2}$  and  $u_{\text{rad}}$  is the radiation energy density, which for simplifying reasons will not be included in the following analytical calculations. It will be however taken into account in our numerical treatment of section 3. Note also that in our analytical formulation we have not included any population of ‘cold’ protons and electrons, which are physically implied by charge conservation arguments. However, their contributions to the total jet power are minor (see for example Protheroe & Mücke 2001) and would not affect our results significantly.

Inserting the expression for  $u_p$  given by equation (25) in the above relation we find that the jet power is a function only of the product  $\delta \cdot B$

$$P_{\text{jet}}^{\text{obs}} = \pi R^2 c \left( \frac{(\delta B)^2}{8\pi} + A(\delta B)^{-3/2} \right). \quad (31)$$

The jet power is minimized when the following condition holds

$$B = (6\pi A)^{2/7} \delta^{-1}. \quad (32)$$

Comparison of equations (26) and (32) shows that whenever the system achieves equipartition the jet power also minimizes at the value

$$P_{\text{jet, min}}^{\text{obs}} = 5.8 \times 10^{47} (L_{\gamma, 48}^{\text{obs}} \ln(\gamma_{\text{max}, 10}))^{\frac{4}{7}} \left( \frac{R_{16}}{\nu_{\gamma, 25}^{\text{obs}}} \right)^{\frac{2}{7}} \text{ erg/s.} \quad (33)$$

Thus, even the minimum jet power obtained in the framework of the proton-synchrotron blazar model is high compared to values inferred from pure leptonic modelling of

blazar emission; see e.g. Celotti & Ghisellini (2008). Since for a large range of  $B$  values the system lies far from equipartition (see figure 1), equations (27) and (32) imply that the calculated jet power differs significantly from its minimum value.

The fact that the Doppler factor has a lower limit implies that for magnetic fields higher than a certain value  $B_h$ , equation (32) cannot be further satisfied and there is no set of parameters that lead to minimization of the jet power. The characteristic value  $B_h$  can be derived by combining equations (24) and (32). It is given by:

$$B_h = 11.6 R_{16}^{-2/3} \lambda^{1/3} \ln(\gamma_{\text{max}, 10})^{1/3} \text{ G.} \quad (34)$$

The same holds also for weak enough magnetic fields. Thus, by combination of equations (15) and (32) one derives a second characteristic value  $B_l$  for the magnetic field, below which there is no set of parameters that could minimize the power of the jet

$$B_l = 0.96 R_{16}^{-4/7} (\nu_{\gamma, 25}^{\text{obs}})^{8/14} \left( L_{\gamma, 48}^{\text{obs}} \ln(\gamma_{\text{max}, 10}) \right)^{-1/7} \text{ G.} \quad (35)$$

Therefore, the discussion above reveals another important physical aspect of  $\delta_{\min}$ ; it limits the range of  $B$ -values among which one should choose in order to obtain the minimum power of the jet. If  $\delta = \delta_{\min}$  the dependence of  $P_{\text{jet}}^{\text{obs}}$  on  $B$  can also be derived by combining equations (15), (24) and (31)

$$P_{\text{jet}}^{\text{obs}}(B; \delta_{\min}) \propto a_1 B^{-4} + a_2 B^3 \quad \text{for } B < B_q \quad (36)$$

and

$$P_{\text{jet}}^{\text{obs}}(B; \delta_{\min}) \propto b_1 B^{12/7} + b_2 B^{-9/7} \quad \text{for } B > B_q, \quad (37)$$

where  $a_{1,2}$  and  $b_{1,2}$  are constants. Note that the functional form of  $P_{\text{jet}}^{\text{obs}}$  is not trivial and it consists of four power-law segments. We will return to this point in the next section, where we perform the numerical approach in fitting the  $\gamma$ -ray observations of 3C 279.

## 3 NUMERICAL RESULTS

In what follows we will present a method of fitting the February 26, 2006 high energy observations of quasar 3C 279 using an one-zone hadronic model. Our working framework is analogous to that adopted in the previous section but with two main differences:

(i) no assumptions about the relative importance of synchrotron cooling with respect to that due to photohadronic processes for the proton distribution are made; particle and photon distributions are self-consistently obtained as the solution to a system of three coupled integrodifferential equations. This is done with the help of the numerical code described in Mastichiadis & Kirk (1995) and Mastichiadis et al. (2005).

(ii)  $\chi^2$  statistics was used to determine which proton-synchrotron spectra provide ‘good’ fits to the VHE  $\gamma$ -ray data.

In order to minimize the number of free parameters we keep fixed the following:  $\gamma_{\min} = 1$ ,  $s = 2$  and  $R = 3 \times 10^{16}$  cm. We note that in the analytical formulation of section 2, we have

used explicitly the parameter  $R$ , although it combines an observable quantity, i.e. the variability timescale  $t_{\text{var}}$  with the Doppler factor  $\delta$ . For this, the derived values of  $\delta$  throughout the present work should be checked *a posteriori* against the relation imposed by the variability of the source

$$\delta \geq \frac{4R_{16}(1+z)}{t_{\text{days}}}, \quad (38)$$

where  $t_{\text{days}}$  is the observed variability timescale normalized to 1 day. One could instead work with the observable  $t_{\text{var}}$  and incorporate this extra constraint in his/her analytical treatment. Possible effects of different adopted values for  $R$  and  $s$  on our results will be discussed in section 4.

### 3.1 The method

Our aim is to produce a parameter space which gives ‘good’ fits to February 2006 observations of 3C 279. Application of existing theoretical models to AGN observations leads to one set of parameters that minimizes the  $\chi^2$ -value. However, the goodness-of-fit may pose some interesting questions, especially when two very different sets of parameters may have very similar values of  $\chi^2$ . For this reason, in what follows, we do not restrict ourselves to the best fit with the minimum  $\chi^2$ -value, but we rather relax the definition of a ‘good’ fit. Thus, fits to the TeV data that have  $\chi_{\text{red}}^2 < 1.5$  are characterized as ‘good’ and they are obtained for different combinations of the parameters. This, as we will show in the next section, results in the formation of a parameter space instead of a single set of accepted parameter values.

Since we keep  $\gamma_{\text{min}}$ ,  $s$  and  $R$  fixed the number of free parameters in the context of a pure hadronic model reduces to four:  $B$ ,  $\gamma_{\text{max}}$ ,  $\ell_p$  and  $\delta$ . Thus, we search for combinations of the aforementioned parameters that provide good fits to the TeV data. At the same time we have treated the X-ray observations as upper limits: As long as the proton induced emission is below the X-ray data, we assume that one can always find a fit to them by using a suitably parametrized leptonic component. On the other hand, if the emission due to photon quenching is above the X-rays, then we discard the fit. The steps of the algorithm followed are

- (i) Choose a value for the magnetic field strength  $B$ .
- (ii) Choose a value for the maximum proton Lorentz factor  $\gamma_{\text{max}}$  starting from the highest possible value, which is imposed by the Hillas criterion (see equation (14)).
- (iii) Choose an injection compactness for the proton distribution  $\ell_p$ . For high enough values, automatic quenching sets in and creates a soft-photon component that exceeds the X-ray observations.
- (iv) Choose a value for the Doppler factor  $\delta$  after taking into account that the variability timescale of 3C 279 does not exceed that of one day.

For each triad  $(B, \gamma_{\text{max}}, \ell_p)$  two values of  $\delta$  can be found that correspond to fits with  $\chi_{\text{red}}^2 \leq 1.5$ . This can be easily explained by the parabolic shape of the  $\chi_{\text{red}}^2$  curves. Figure 2 shows  $\chi_{\text{red}}^2$  as a function of  $\delta$  for  $B = 40$  G and  $\gamma_{\text{max}} = 4 \times 10^9$ . Different curves correspond to different values of  $\ell_p$ . The part of the curve that lies below the horizontal line with  $\chi_{\text{red}}^2 = 1.5$  provides good fits. Its projection on the horizontal axis defines an interval of  $\delta$ -values. For simplifying reasons, we consider that each monotonic branch of the

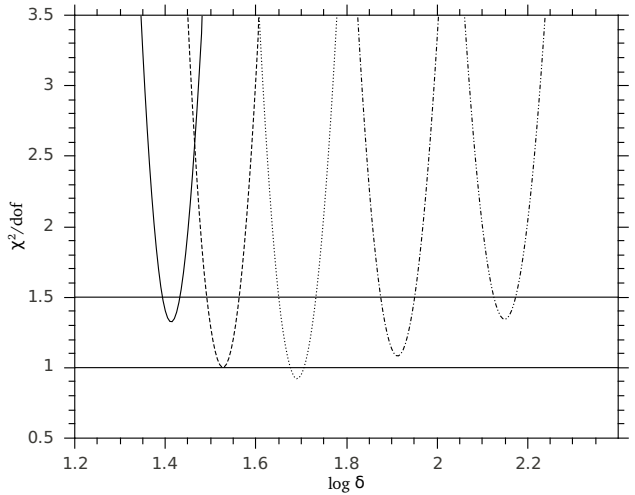


**Figure 2.** Reduced  $\chi^2$  as a function of the Doppler factor  $\delta$  for  $B = 40$  G,  $\gamma_{\text{max}} = 4 \times 10^9$  and  $\ell_p = 10^{-8}$  (solid line),  $\ell_p = 10^{-7}$  (dashed line),  $\ell_p = 10^{-6}$  (dotted line),  $\ell_p = 6.3 \times 10^{-6}$  (dashed-dotted line) and  $\ell_p = 2.5 \times 10^{-5}$  (dashed-double dotted line). The horizontal solid line with  $\chi_{\text{red}}^2$  shows the upper limit below which a fit is characterized as ‘good’. The line  $\chi_{\text{red}}^2 = 1$  is also shown.

$\chi_{\text{red}}^2$ -curve that lies below the horizontal line is represented only by one  $\delta$ -value, i.e. only by one point on the horizontal axis. Thus, for each  $\ell_p$  we find two representative values of the Doppler factor. The error we make in this case is not large since the curves are very steep. Note also that Doppler factors lying between the two representative  $\delta$ -values also provide good fits. If we repeat the above procedure for various  $\gamma_{\text{max}}$  we can then create a parameter space for  $\ell_p$  and  $\delta$  for a specific value of the  $B$ -field. An example is shown in figure 3 for  $B = 40$  G and different  $\gamma_{\text{max}}$ . For the case considered here,  $\gamma_{\text{max}}$  ranges from  $10^{9.6}$  (horizontally dashed area) to  $10^{10}$  (vertically dashed area) with a step of 0.2 in logarithmic units. The envelope of each striped area is the result of the two representative values of  $\delta$  defined for each  $\ell_p$ , as previously described. Note that in a log-log plot the lines of the envelope are power laws with an exponent  $-0.22$ , i.e.  $\delta \propto \ell_p^{-0.22}$ . This almost coincides with the value  $-2/7$  found in our analytical approach (see equation 13). Values of  $\gamma_{\text{max}}$  outside this range do not provide good fits and are therefore discarded. Thus, the shaded areas in Figure 3 depict all the possible combinations of  $\ell_p$ ,  $\gamma_{\text{max}}$  and  $\delta$  that provide good fits to the TeV observations. We note that one can use low values of the proton injection compactness  $\ell_p$  and get acceptable TeV fits but this can be done only if he/she allows the Doppler factor to take high values – this is due to the fact that the observed and blob frame luminosities are related by  $L_{\text{obs}} \propto \delta^4 L_{\text{int}}$ , while  $L_{\text{int}} \propto L_p \propto \ell_p$ . On the other hand, higher values of  $\ell_p$  naturally result in lower  $\delta$  values. However, as stated earlier, we find that  $\gamma$ -ray quenching plays an important role when  $\ell_p$  takes higher values. In this case the spontaneously produced soft photons increase and eventually will start violating the X-ray observations, destroying the goodness of the fit. Therefore, an upper limit is imposed on the allowed values of  $\ell_p$  which implies in turn, the existence of a minimum value of the Doppler factor (see equations (23) and (24)).

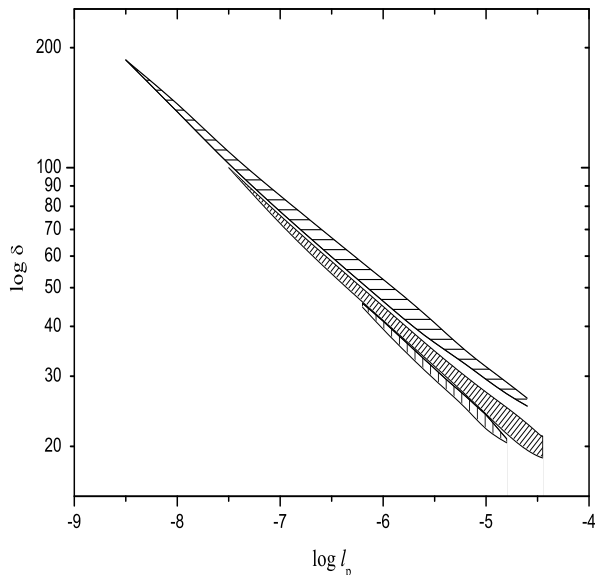


**Figure 3.** Parameter space of pairs  $(\ell_p, \delta)$  for  $B = 40$  G and different  $\gamma_{\max}$  that correspond to TeV fits with reduced  $\chi^2 < 1.5$ . Each shaded area corresponds to a different value of  $\gamma_{\max}$  that ranges from  $10^{9.6}$  to  $10^{10}$  with a step of 0.2 in logarithmic units. For each value of  $\ell_p$  two values of  $\delta$  can be determined, which form the envelope of each striped area. The shaded areas enclosed by the solid lines correspond also to values of  $(\ell_p, \delta)$  for which good fits to the TeV data ( $\chi_{\text{red}}^2 < 1.5$ ) can be obtained.

### 3.2 Minimum Doppler factor

Figure 4 exemplifies the effect of  $\gamma$ -ray absorption on the adopted values of  $\ell_p$  and  $\delta$  for fitting the TeV data. The MAGIC TeV data points show the measured flux corrected for intergalactic  $\gamma\gamma$  absorption. The lowest possible level of extragalactic background light (EBL) according to Primack et al. (2005) has been used for the de-absorption of the VHE  $\gamma$ -rays. The full line curve depicts the last good-fit spectrum we obtain for a high  $\ell_p$ . Here  $\ell_p = 4 \times 10^{-5}$ ,  $\gamma_{\max} = 10^{9.8}$  and  $\delta_{\min} = 18.6$ . Other parameters used for this plot are:  $\gamma_{\min} = 1$ ,  $R = 3 \times 10^{16}$  cm,  $B = 40$  G and  $s = 2$ . Note first that the minimum Doppler factor derived here does not violate the inequality (38) for  $t_{\text{days}} = 1$ , and second that  $B^2\gamma_{\max}$  satisfies the constraint given by relation (6). The non-linear cascade due to quenching has produced a soft component that is almost at the observed X-ray flux. Any attempt to increase  $\ell_p$  further will produce a higher flux of soft photons which would violate the X-rays. To demonstrate this point further, we have ran the code for a high value of  $\ell_p = 10^{-3}$ . This value is well inside the quenching regime and thus should be excluded due to strong X-ray production. However, by turning artificially  $\gamma\gamma$  absorption off, we inhibit the growth of the non-linear cascade and therefore a good fit can be obtained with a  $\delta$  as low as 10 (dashed line). Moreover, if  $\gamma\gamma$  absorption is treated in an approximate semi-analytic manner as a linear absorption process, automatic quenching of  $\gamma$ -rays will not even occur, since it is a purely non-linear absorption process. Therefore, no

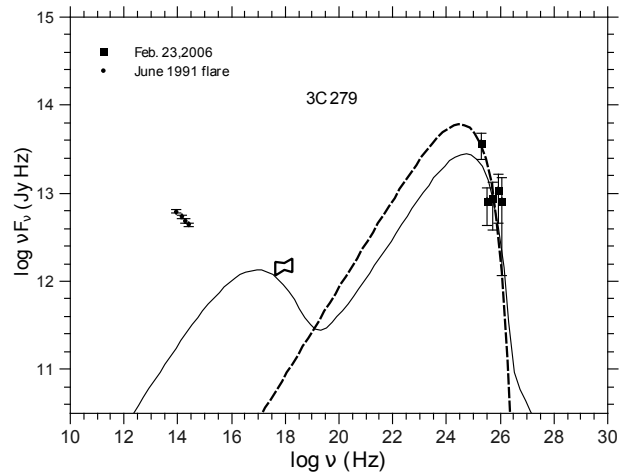


**Figure 4.** Multiwavelength spectra of 3C 279 in the context of a pure hadronic model for  $R = 3 \times 10^{16}$  cm,  $B = 40$  G,  $\gamma_{\min} = 1$ ,  $\gamma_{\max} = 6.3 \times 10^9$  and  $s = 2.0$ . The solid curve is obtained with all processes taken into account for  $\ell_p = 10^{-4.4}$  and  $\delta_{\min} = 18.6$ , whereas the dotted one is obtained for  $\ell_p = 10^{-3}$  and  $\delta = 10$  after artificially ignoring  $\gamma\gamma$  absorption. Squares represent the VHE-detection by MAGIC (Albert et al. 2008) after correcting for intergalactic  $\gamma\gamma$  absorption, the bowtie represents the Swift data and filled circles are IR data during the flare of June 1991 taken by (Hartman et al. 1996).

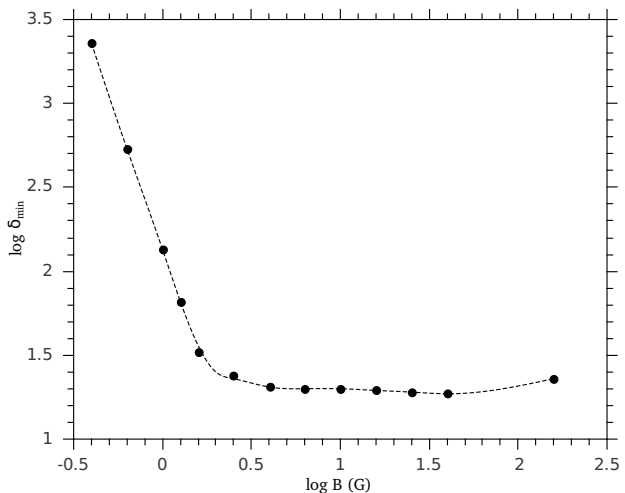


**Figure 5.** Minimum value of the Doppler factor  $\delta_{\min}$  (points) as a function of the magnetic field strength  $B$ . The dashed line is the result of spline interpolation between the points.

limiting value of the proton and  $\gamma$ -ray compactness would be found and the transition of the hadronic system to supercriticality would not be seen. As a result one would find erroneously a more extended parameter space that fits the data. In such case, the Doppler factor would not be limited to a lower value apart from the one found by the usual gyroradius arguments made in section 2.

As a next step we have obtained  $\delta_{\min}$  for various values of the magnetic field  $B$ . This is depicted in figure 5, where the two branches derived analytically in the previous section (see figure 1) are clearly seen. The power law dependence of  $\delta_{\min}$  on  $B$  can be modelled as of  $\delta_{\min} \propto B^{-\alpha}$  with



$\alpha \simeq 2.85$  for the *low-B* branch and  $\alpha \simeq 0.05$  for the *high-B* branch. We note that the numerically derived power-law exponents of the two branches are very close to those given by equations (15) and (24) respectively. A new feature of figure 5 is that for very strong magnetic fields, where synchrotron cooling affects a significant part of the proton power-law distribution, the minimum Doppler factor required for a good fit slightly increases with increasing  $B$ .

### 3.3 Energetics

The previous analysis makes evident that acceptable fits to the TeV observations of 3C 279, within the context of the hadronic model, can be found for a large choice of magnetic fields, maximum proton energies and injection luminosities. We note also that these values are similar to the ones found in standard hadronic modelling of TeV sources (Böttcher et al. 2009).

Having already derived  $\delta_{\min}$  for each magnetic field strength, we numerically then derive the steady state proton energy density  $u_p^* \equiv u_p(\delta_{\min}(B))$  and plot this quantity as a function of  $B$  – see figure 6. The system becomes magnetically dominated either for high enough ( $B > 10$  G) or low enough ( $B < 0.7$  G) magnetic fields. These values should be compared to  $B_h$  and  $B_l$  given by equations (34) and (35) respectively. The two curves intersect at two points, exactly as was analytically derived (see section 2.2). At these points the two energy densities are equal and this corresponds to a minimum of the total energy density, i.e. to an equipartition between the particles and the magnetic field – we emphasize that the quantity  $u_p^*$  is not the minimum particle energy density. The fact that  $\delta_{\min}$  has a strong dependence on  $B$  at low values is also reflected to  $u_p^*$ . Our analytical result given by equation (28) should be compared to the numerical one, i.e.  $u_p^* \propto B^{8.7}$ . For  $B > 2$  G (c.f.  $B_q$  of equation 27) the particle energy density decreases with increasing magnetic field as  $B^{-1.4}$ . This trend was also found analytically. The power-law exponent however is slightly different – see equation (29).

From equation (30) and for  $\delta = \delta_{\min}(B)$  and  $\ell_p = \ell_p(\delta_{\min})$  we have calculated numerically the observed jet power, which becomes a function only of the magnetic field, i.e.  $P_{\text{jet}}^{\text{obs}}(\delta_{\min}(B))$ . This is shown in figure 7. The function  $P_{\text{jet}}^{\text{obs}}(\delta_{\min}(B))$  shows two local minima for two values of the magnetic field that differ more than one order of magnitude. For a wide range of  $B$  values the calculated jet power is rather high  $\approx 10^{48} - 10^{49}$  erg/s in comparison to leptonic models (Celotti & Ghisellini 2008). In a log-log plot the curve consists of four distinct power-law segments labeled with the numbers 1 to 4. In Table 1 the power-law exponents of the four segments and the corresponding analytically derived values given by equations (36) and (37) are listed. Apart from the first segment both results are in good agreement.

We have already shown that the jet power minimizes whenever  $\delta$  and  $B$  satisfy equation (32). In this case the system is close to a state of equipartition. We proceed to investigate whether these results are verified numerically. For each value of  $B$ , we therefore search among the triads  $(\gamma_{\text{max}}, \ell_p, \delta)$  found during the fitting process for that specific set of values that minimizes the jet power. Figures 8 and 9 show respectively the minimum calculated jet power  $P_{\text{jet},\min}^{\text{obs}}$

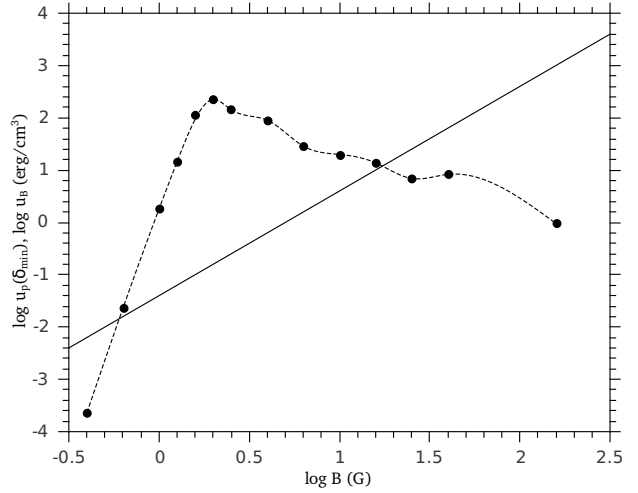


**Figure 6.** Logarithmic plot of the proton energy density in the case of the minimum Doppler factor  $u_p^*$  (points) and of the magnetic energy density (solid line) as a function of the magnetic field. Spline interpolation between the points results in the dashed line.

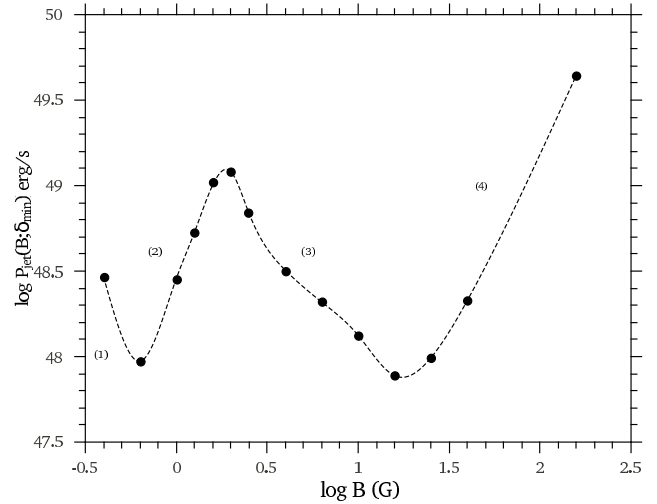


**Figure 7.** Jet power as a function of the magnetic field for  $\delta = \delta_{\min}$  (points). The dashed line is the result of spline interpolation. Numbers label the different power-law segments of the curve.

Number of segment	exponent	
	numerical	analytical
(1)	-2.50	-4.00
(2)	+2.30	+3.00
(3)	-1.30	-1.28
(4)	+1.70	+1.71

**Table 1.** Power-law exponent of  $P_{\text{jet}}^{\text{obs}}(\delta_{\min}(B))$  as derived from the numerical and analytical treatment.



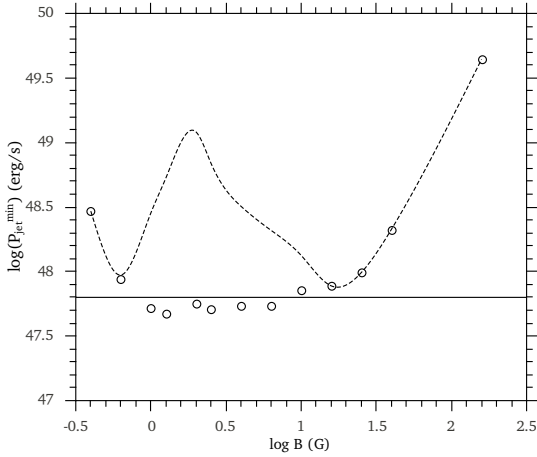


**Figure 8.** Minimum jet power value (open circles) as a function of the magnetic field strength. The horizontal line denotes the analytically derived minimum value of the jet power (equation 33) and the dashed line, which is same as in figure 7, is shown for comparison reasons. Open circles that lie on the dashed line correspond to the jet power calculated for  $\delta_{\min}$ , since  $\delta < \delta_{\min}$  would be required to minimize the jet power.

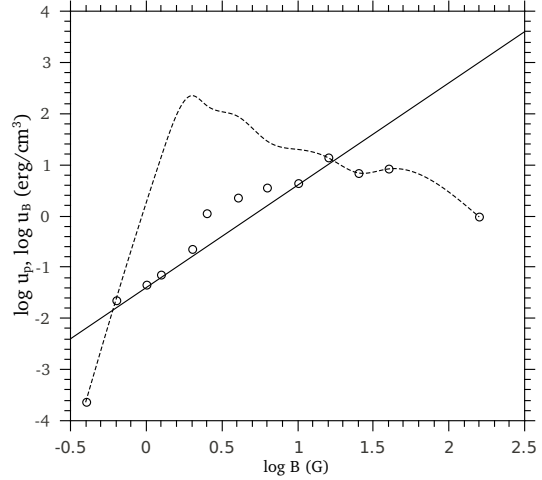
and the corresponding proton energy density as a function of  $B$ . Dashed lines are same as in figures 6 and 7 and are shown for comparison reasons.

Figure 8 shows that for  $0.7 \leq B \leq 10$  G all points lie close to the minimum value  $P_{\text{jet,min}}^{\text{obs}} \simeq 6.5 \times 10^{47}$  erg/s, whereas for  $B > 10$  G and  $B < 0.7$  G the minimum jet power found from our numerical data sets coincides with that calculated for  $\delta = \delta_{\min}$  (open circles lying on the dashed line). As already discussed in section 2.3 the jet power calculated in this case is not the lowest possible minimum value, since this would be obtained for Doppler factors less than  $\delta_{\min}$ . Note that the transitions occur at  $B \approx B_1 \approx 0.7$  G and  $B \approx B_h \approx 10$  G.

In figure 9 one can see that  $u_p \approx u_B$  for  $B_1 \leq B \leq B_h$ , which is in complete agreement with the analytical estimates of section 2.3. The fact that the calculated jet power is not the minimum possible one, can also be verified by the fact that the system for  $B > 10$  G and  $B < 0.7$  G is far from an equipartition state.

Each of the points shown as open circles in figures 8 and 9 corresponds to a set of parameters  $(B, \gamma_{\text{max}}, \ell_p, \delta)$  with  $\delta \geq \delta_{\min}$ , for which the jet power is actually the minimum possible in the context of a hadronic model. In figure 10 we plot the ratio  $\delta/\delta_{\min}$  against the magnetic field strength. For the range  $0.7 < B \leq 10$  G where the system is close to equipartition and the power of the jet is minimum, the ratio becomes larger than unity.

The conclusions drawn from the figures of the present section can be summarized as follows: if one chooses to model the VHE  $\gamma$ -ray spectra using values of  $(B, \gamma_{\text{max}}, \ell_p, \delta)$  that minimize both the required jet power and the total energy density of the system, i.e. model the system using optimum energetic conditions, then one will be confronted with the requirement of a high Doppler factor. On the other hand, acceptable fits of the TeV data using the minimum possible Doppler factor lead to a particle dominated system



**Figure 9.** Proton energy density (open circles) as a function of the magnetic field strength, for those parameter sets that correspond to the minimum jet power. The magnetic field energy density is shown with the solid line. The remaining symbols are the same as in figure 8.

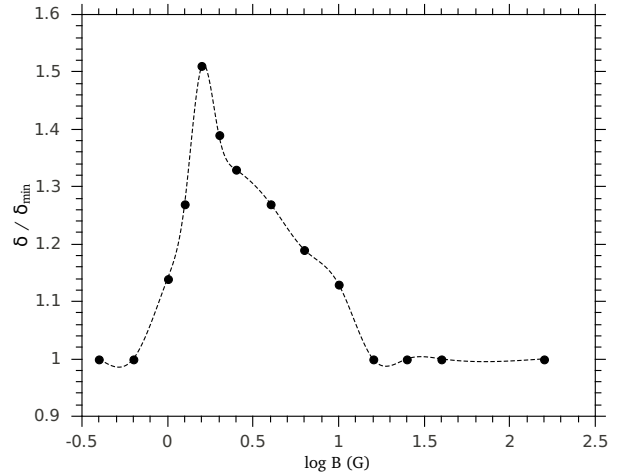


**Figure 10.** Ratio  $\delta/\delta_{\min}$  as a function of the magnetic field. Here  $\delta$  is the Doppler factor required for minimization of the jet power. Interpolation between the points results in the dashed line.

and to high values of  $P_{\text{jet}}^{\text{obs}}$  for a wide range of  $B$  values, i.e. the energetic requirements in this case are higher.

#### 4 EFFECTS OF OTHER PARAMETERS

In our numerical treatment we have kept fixed to specific values the power-law index of the injected proton distribution, the radius of the emitting blob as well as the energy of the  $\gamma$ -ray photons  $\epsilon_{\gamma}^{\text{obs}}$ . Here we discuss possible effects of different adopted values on our results, since our initial assumption could be critical for exploring the whole physically allowed parameter space for the system of 3C 279 at the observed state.

#### 4.1 Power-law index $s$

Throughout the present work we have assumed that the proton distribution is a power law of exponent  $s = 2$ . In this case the energy per logarithmic interval is the same. A different adopted value would affect the proton energy density quantitatively and therefore our energetics estimates. Let us for example consider a steep power law distribution with  $s > 2$ . In this case more energy is injected to the protons with the minimum Lorentz factor, whereas protons at the upper cutoff of the distribution, which are responsible for the emitted radiation, carry only a small fraction of the energy. Thus, for the same proton injection compactness the total number  $N_p$  and consequently the energy density of protons  $u_p$  increases with increasing  $s$ . In addition, the calculated  $\gamma$ -ray compactness for the same  $\ell_p$  is lower. Thus, a larger proton compactness  $\ell_p$  and therefore energy density would be required in order to fit the TeV observations with the same Doppler factor. As an extreme example, we considered a very steep proton distribution with the highest value for the power law exponent predicted by acceleration theory, i.e.  $s = 2.5$ . The fit to the TeV observations was obtained using:  $B = 40$  G,  $\delta \approx 25$  and  $\ell_p = 10^{-1.3}$ . The proton energy density in this case is  $u_p = 10^4$  erg/cm $^{-3}$ , which is much higher than the values presented in section 3.3. Therefore, the case of a flat proton distribution is rather conservative as far as the energetics is concerned.

#### 4.2 Radius of the emitting region

The fact that there is a very good agreement between the numerical results and our analytical expressions, where the dependence on  $R$  is explicit, makes possible the prediction of the effects of a different adopted value on our results. Let us assume a more compact source with  $R = 3 \times 10^{15}$  cm. The quantities that are directly affected by a change in the source size are listed below in descending order in terms of their dependence on  $R$ :

(i) The minimum Doppler factor for  $B < B_q$  (see equation 15), which would be increased by two orders of magnitude. Therefore, the ‘steep’ branch of the plot in figure 5 would be shifted upwards by a factor of two in logarithmic scale. Note, that the constraint set by variability arguments (relation 38) will not be violated since it implies an even lower limit to the Doppler factor than previously.

(ii) The equipartition magnetic field  $B_{eq}$  given by equation (27), which for a certain  $\delta$  will be increased by a factor of 7.

(iii) The magnetic field above which the feedback criterion is satisfied. We remind that the scaling of  $B_q \propto R^{-3/5}$  has been derived after taking into account the constraint of the Hillas criterion on  $\gamma_{max}$ .

(iv) The minimum Doppler factor set by the automatic quenching is rather insensitive to changes of  $R$  and it would be increased just by a factor of 2 (see equation (24)).

The proton energy density as well as the jet power calculated in the case of a blob moving with  $\delta = \delta_{min}$  will be also affected by a change in  $R$ . We remind that  $u_p \propto R^{-3}\delta^{-7/2}$

(see equation 25); the dependence on  $R$  comes through the constant  $A$ . Taking into account points (i) and (iv) above, we find that  $u_p(\delta_{min}) \propto R^4$  for  $B < B_q$  and  $u_p(\delta_{min}) \propto R^{-4}$  for  $B > B_q$ . Since  $B_q$  also increases by a factor of 4, one expects to find significantly smaller values for  $u_p(\delta_{min})$  than those shown in figure 6 for a wider range of B-values (up to  $\simeq 14$  G). The jet power obtained in this case has also a strong dependence on  $R$ , which is embedded in the constants  $\alpha_{1,2}$  and  $b_{1,2}$  of equations (36) and (37) respectively. More specifically one finds that  $\alpha_1 \propto R^{-2}$  and  $\alpha_2 \propto R^2$  whereas  $b_1 \propto R^{10/7}$  and  $b_2 \propto R^{-4/7}$ . The shape of the curve shown in figure 7 would be transformed by shifting the different power-law segments vertically and horizontally, since the values of the magnetic field where the local minima occur would also be affected (see equations 34 and 35). It is important, however, to note that the minimum Doppler factor in this case would be extremely high (see also point (i) above). This makes the scenario of a more compact  $\gamma$ -ray emitting region for 3C 279 less plausible.

#### 4.3 Energy of $\gamma$ -ray photons

Another question that naturally arises is how our results would change if the fitting method was used for another set of  $\gamma$ -ray observations, e.g. in the GeV regime. Note that some recent contemporary  $\gamma$ - and X-ray observations of 3C 279 (e.g. Abdo et al. 2010; Hayashida et al. 2012) could be an interesting case. In principle, the method outlined in sections 2 and 3 can be applied with the only difference that the effects of quenching will not be seen, as automatic quenching cannot set in for lower  $\gamma$ -ray energies at least for typical magnetic field strengths. This is exemplified in figure 11, where characteristic values of the magnetic field are plotted against  $\gamma_{max}$  in the extreme case of  $\delta = 1$ . Specifically, the thick solid line corresponds to  $B_q$  (see equation (19)) and divides the parameter space into two regions. For  $B$  values that lie above this line, the feedback criterion is satisfied. The thin solid line corresponds to the Hillas criterion, i.e.  $B \geq (m_p c^2 / eR) \gamma_{max}$ . Therefore, the parameter space below this line is not allowed. Finally, the thin and thick dotted lines show the locus of  $B$  and  $\gamma_{max}$  values, that correspond to  $\epsilon_{\gamma}^{obs}$  equal to 0.1 TeV and 1 GeV respectively, i.e.  $B = \epsilon_{\gamma}^{obs} (m_p c / \hbar e) \gamma_{max}^{-2} \delta^{-1}$  for  $\delta = 1$ . Therefore, in the case where GeV observations were used, one would need extremely high values of the magnetic field, in order to see the effects of automatic quenching. These would be even higher if one would take into account the exact value of the Doppler factor.

## 5 DISCUSSION

Hadronic models have been used extensively for fitting the  $\gamma$ -ray emission from Active Galactic Nuclei. Usually, detailed fitting to the multiwavelength spectrum of these objects requires, in addition to a population of relativistic protons, the presence of an extra leptonic component which is responsible for the emission at lower energies (radio to UV or X-rays).

As it was shown recently (Stawarz & Kirk 2007; Petropoulou & Mastichiadis 2011, 2012) compact  $\gamma$ -ray

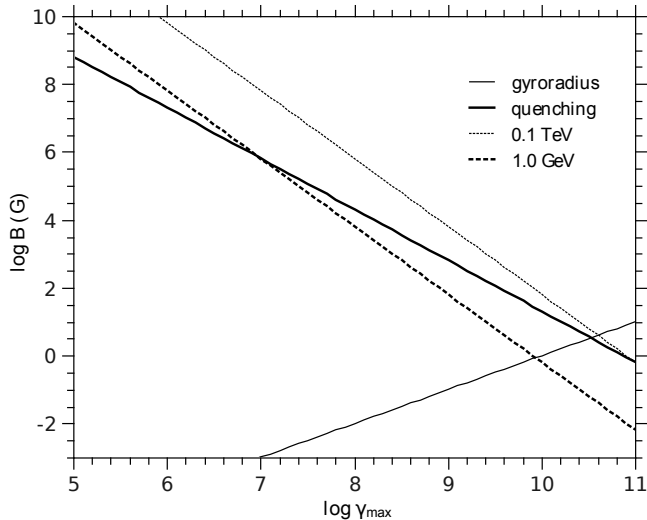


**Figure 11.** Log-log plot of characteristic values of the magnetic field against the maximum proton Lorentz factor. The space below the thin solid line is not allowed, since it violates the Hillas criterion. The feedback criterion is satisfied for values of  $B$  and  $\gamma_{\max}$  that lie above the thick solid line, which represents  $B_q$ . Finally, the thin and thick dotted lines  $B$  and  $\gamma_{\max}$  values, that correspond to  $\epsilon_{\gamma}^{\text{obs}}$  equal to 0.1 TeV and 1 GeV respectively.

sources can be subject to photon quenching which can result, if certain conditions are met, to automatic  $\gamma$ -ray absorption and redistribution of the absorbed  $\gamma$ -ray luminosity to electron-positron pairs and lower energy radiation. This is a non-linear loop which can operate even in the absence of an initial soft photon population and is expected to have direct consequences on the aforementioned models. For the present application other feedback loops, such as the Pair-Production-Synchrotron one (Kirk & Mastichiadis 1992), are less relevant as they usually operate at lower proton energies and at higher energy densities (Dimitrakoudis et al. 2012).

Aim of the present paper is to set a general framework for investigating the effects of photon quenching on the parameter space available for modelling  $\gamma$ -rays in the context of a hadronic model. As an example we concentrated on the February 2006 observations of the blazar 3C 279 which were performed simultaneously in the TeV and X-ray regimes. To this end we have focused only on fitting the high energy spectrum using a synchrotron proton emission and treating conservatively the X-ray observations as an upper limit. We found that for a wide range of parameters, automatic photon quenching plays a crucial role as its onset produces X-rays which violate the observations. To be able to assess its impact on the parameter space, we have relaxed the usual goodness-of-fit method by accepting fits with  $\chi_{\text{red}}^2 < 1.5$ . Our results indicate, in agreement with other researchers in the field, that the hadronic model requires in general high magnetic fields. Additionally we find that the presence of automatic quenching limits the proton luminosity (or, equivalently the proton energy density in the case of non substantial proton cooling) which, in turn, results in a minimum value of the Doppler factor  $\delta_{\min}$ . Interestingly enough, these ideas do not apply to leptonic models because they favour

much lower values for the magnetic field. For these values photon quenching does not operate, since its feedback criterion is not satisfied. The latter is a necessary condition for the emergence of automatic quenching and requires for a given  $\gamma$ -ray energy a certain value of the magnetic field  $B_q$ , for the absorption loop to operate. We have shown both analytically and numerically, (see figures 1 and 5 respectively), that the minimum Doppler depends on the magnetic field strength in a different way, depending on the relative relation of  $B$  and  $B_q$ . Specifically, if the magnetic field strength is above  $B_q$ , then  $\delta_{\min} \propto B^{-1/7}$ . For values of the magnetic field with  $B < B_q$  quenching is not relevant. However, we have shown using arguments based on the particles gyroradii, that also in this case a lower limit to the Doppler factor exists, which depends strongly on  $B$ , i.e.  $\delta_{\min} \propto B^{-3}$ . Therefore if one wants to adopt a low magnetic field for the radiating region, fits to the TeV  $\gamma$ -rays are still possible but at the expense of a very high value of the Doppler factor.

The fact that quenching does not allow the Doppler factor to become smaller than some value is intriguing and leads naturally to the investigation of the proton energy density inside a blob which moves with this characteristic value. In this case, we showed that there are two values of the magnetic field that minimize the energy content, one corresponding to the  $\delta$  branch with  $B < B_q$  and the other to the one with  $B > B_q$ . For values of the magnetic field between the two equipartition magnetic fields, the emission region is particle dominated and the ratio  $u_p/u_B$  can be as large as  $10^3$  (see figure 6). Note however, that if a Doppler factor twice the minimum one is adopted, then the calculated proton energy density for the same magnetic field will be lower by almost an order of magnitude – see equation (12). Furthermore, we have calculated the jet power in the case where  $\delta = \delta_{\min}$  and shown both analytically and numerically that it is a function of  $B$ . The jet power is rather high ( $10^{47} - 10^{49}$  erg/sec) for the whole range of  $B$  values, as expected in the context of hadronic modelling.

We have repeated the above calculations by relaxing the condition  $\delta = \delta_{\min}$  while requiring the parameters to be such as to minimize the power of the jet. In this case we have shown that the energy content of the blob is also minimized (see figures 8 and 9). For adopted  $B$  values lying between the two equipartition values, the jet power can be minimized, albeit at the cost of a high  $\delta$  value. However, we have shown that for magnetic field values outside of this range, jet power minimization is not possible as this can be achieved only if  $\delta < \delta_{\min}$ . Thus, the existence of a minimum value for  $\delta$  has indirect implications on the energetics of the system.

An interesting question is whether a detailed fitting to the X-ray observations of 3C 279 with the addition of an extra leptonic component would bring any change to the basic ideas presented here. In this case apart from automatic quenching, the linear absorption of  $\gamma$ -rays on the X-ray photons emitted by the leptonic component, is also at work. However, by including this component and repeating our numerical calculations of §3, we found that our results do not change. This is due to the fact that the X-ray luminosity of 3C 279 is rather low and therefore the effects of linear  $\gamma\gamma$  absorption are minimal, at least up to the compactnesses above which the automatic photon quenching sets in. Apart from the absorption of  $\gamma$ -rays on the synchrotron photons

emitted by the ‘extra’ leptonic component discussed above, inverse Compton scattering of these photons to higher energies by the same leptonic component would be an additional mechanism at work. The upscattered photons would lie in the hard X-ray and  $\gamma$ -ray energy range and would affect our calculations only if their luminosity  $L_{\text{SSC}}$  would be comparable to that carried by the synchrotron component  $L_{\text{syn}}$ . While estimating the ratio  $u_{\text{syn}}/u_{\text{B}}$  for a wide range of  $B$  and  $\delta_{\text{min}}$  values used in the present work (see figure 5) we find that this is always much smaller than unity, and therefore the inverse Compton scattering of an extra leptonic component which would fit the radio to X-ray observations does not interfere to the quenching mechanism.

The estimation method proposed in the present work can be regarded as an extension of the widely used method for estimating the equipartition magnetic field using radio observations. In our case, the leptonic synchrotron component is replaced by the proton synchrotron emission and the radio by the VHE  $\gamma$ -ray observations. The innovative feature of our method is the estimation of a minimum Doppler factor, which is the result of automatic photon quenching. This can be more of relevance to TeV observations rather than the Fermi ones as quenching at GeV energies requires very high values of the magnetic field – see figure 11. The fact that our numerical results are in very good agreement with the analytical calculations offers a fast yet robust way for estimating many physical quantities of the  $\gamma$ -ray emitting region of TeV blazar jets. We caution however the reader, that the effects of automatic quenching, i.e. when no soft photons are initially present in the emitting region, can be seen only in a self-consistent treatment of the radiative transfer problem.

## 6 ACKNOWLEDGEMENTS

This research has been co-financed by the European Union (European Social Fund – ESF) and Greek national funds through the Operational Program “Education and Lifelong Learning” of the National Strategic Reference Framework (NSRF) - Research Funding Program: Heracleitus II. Investing in knowledge society through the European Social Fund. We would like to thank Dr. Anita Reimer and the anonymous referee for useful comments on the manuscript.

## REFERENCES

- Abdo A. A. et al., 2010, *Nature*, 463, 919  
 Albert J. et al., 2008, *Science*, 320, 1752  
 Böttcher M., Reimer A., Marscher A. P., 2009, *ApJ*, 703, 1168  
 Celotti A., Ghisellini G., 2008, *MNRAS*, 385, 283  
 Chatterjee R. et al., 2008, *ApJ*, 689, 79  
 Dermer C. D., Schlickeiser R., 1993, *ApJ*, 416, 458  
 Dermer C. D., Schlickeiser R., Mastichiadis A., 1992, *A&A*, 256, L27  
 Dimitrakoudis S., Petropoulou M., Mastichiadis A., 2012, *International Journal of Modern Physics Conference Series*, 8, 19  
 Harris D. E., Krawczynski H., 2002, *ApJ*, 565, 244  
 Hartman R. C. et al., 1996, *ApJ*, 461, 698  
 Hayashida M. et al., 2012, *ArXiv e-prints*  
 Hillas A. M., 1984, *ARAA*, 22, 425  
 Kirk J. G., Mastichiadis A., 1992, *Nature*, 360, 135  
 Mannheim K., Biermann P. L., 1992, *A&A*, 253, L21  
 Maraschi L., Ghisellini G., Celotti A., 1992, *ApJ*, 397, L5  
 Mastichiadis A., Kirk J. G., 1995, *A&A*, 295, 613  
 Mastichiadis A., Protheroe R. J., Kirk J. G., 2005, *A&A*, 433, 765  
 Mücke A., Protheroe R. J., 2001, *Astroparticle Physics*, 15, 121  
 Mücke A., Protheroe R. J., Engel R., Rachen J. P., Stanev T., 2003, *Astroparticle Physics*, 18, 593  
 Murase K., Dermer C. D., Takami H., Migliori G., 2012, *ApJ*, 749, 63  
 Pacholczyk A. G., 1970, *Radio Astrophysics*  
 Petropoulou M., Mastichiadis A., 2011, *A&A*, 532, A11+  
 Petropoulou M., Mastichiadis A., 2012, *MNRAS*, 421, 2325  
 Primack J. R., Bullock J. S., Somerville R. S., 2005, in *American Institute of Physics Conference Series*, Vol. 745, *High Energy Gamma-Ray Astronomy*, Aharonian F. A., Völk H. J., Horns D., eds., pp. 23–33  
 Protheroe R. J., Mücke A., 2001, in *Astronomical Society of the Pacific Conference Series*, Vol. 250, *Particles and Fields in Radio Galaxies Conference*, Laing R. A., Blundell K. M., eds., p. 113  
 Stawarz Ł., Kirk J. G., 2007, *ApJ*, 661, L17  
 Tavecchio F., Ghisellini G., Bonnoli G., Foschini L., 2011, *MNRAS*, 414, 3566